Experimental and theoretical investigation of FeCrVAl and related compounds

Pavel V. Lukashev, ¹ Lukas Stuelke, ¹ Zach Pottebaum, ¹ Young Moua, ¹ Gavin Baker, ² Jax Wysong, ² Matthew Flesche, ² Shah Valloppilly, ³ Paul M. Shand, ¹ and Parashu Kharel ²

Abstract

We have carried out a combined theoretical and experimental investigation of FeCrVAl, and the effect of Mn and Co doping on its structural, magnetic, and electronic band properties. Our first principles calculations indicate that FeCrVAl, FeCr_{0.5}Mn_{0.5}VAl, and FeCr_{0.5}Co_{0.5}VAl exhibit nearly perfect spin polarization, which may be further enhanced by mechanical strain. At the same time, FeCrV_{0.5}Mn_{0.5}Al and FeCrV_{0.5}Co_{0.5}Al exhibit a relatively small value of spin polarization, making them less attractive for practical applications. Using arc melting and high vacuum annealing, we synthesized three compounds FeCrVAl, FeCr_{0.5}Mn_{0.5}VAl, and FeCr_{0.5}Co_{0.5}VAl, which are predicted to exhibit high spin polarization. The room temperature x-ray diffraction patterns of all samples are fitted with full B2 type disorder with a small amount of FeO₂ secondary phase. All samples show very small saturation magnetizations at room temperature. The thermomagnetic curves M(T) of FeCrVAl and FeCr_{0.5}Co_{0.5}VAl are similar to that of a paramagnetic material, whereas that of FeCr_{0.5}Mn_{0.5}VAl indicates ferrimagnetic behavior with the Curie temperature of 135 K. Our findings may be of interest for researchers working on Heusler compounds for spin-based electronic applications.

I. Introduction

Half metallic Heusler alloys are among the most studied compounds for the device applications in spintronics. In addition to potentially providing a perfect 100% spin polarization, they often exhibit a Curie temperature much higher than the room temperature, which makes them particularly attractive for device applications. ^{1,2,3,4,5,6,7} In addition to half-metallicity, Heusler compounds may exhibit other physical phenomena of practical importance, such as perpendicular

¹Department of Physics, University of Northern Iowa, Cedar Falls, IA 50614, USA

²Department of Physics, South Dakota State University, Brookings, SD 57007, USA

³ Nebraska Center for Materials and Nanoscience, University of Nebraska, Lincoln, NE 68588, USA

magnetic anisotropy, shape memory effect, spin-gapless semiconductivity, etc. 8,9,10,11 At the same time, materials predicted (usually from density functional calculations) to be half-metallic may exhibit reduced spin polarization in practice. In particular, atomic disorder and surface states in thin-film geometry are typically reported to reduce the degree of spin polarization. 12,13,14,15,16,17,18,19 It has been also reported that half-metallicity could be restored in thin-film geometry by interface engineering. 20,21

Here, we present results of our combined experimental and theoretical study of FeCrVAl and related compounds, namely, FeCr_{0.5}Mn_{0.5}VAl, FeCr_{V_{0.5}}Mn_{0.5}Al, FeCr_{0.5}Co_{0.5}VAl and FeCrV_{0.5}Co_{0.5}Al. The parent compound has been predicted to exhibit half-metallicity.²² Our calculations indicate that FeCrVAl, FeCr_{0.5}Mn_{0.5}VAl, and FeCr_{0.5}Co_{0.5}VAl exhibit nearly perfect spin polarization. In addition, mechanical strain may be used to further enhance the spin polarization of the first two compounds. At the same time, FeCrV_{0.5}Mn_{0.5}Al and FeCrV_{0.5}Co_{0.5}Al exhibit small values of spin polarization, making them unattractive for practical spintronic applications. Since only three compositions FeCrVAl, FeCr_{0.5}Mn_{0.5}VAl, and FeCr_{0.5}Co_{0.5}VAl exhibit nearly perfect spin polarization, we have synthesized these compounds and studied their structural and magnetic properties.

The rest of the paper is organized as follows. In Section II, we outline the experimental and computational methods. Section III contains our results; it consists of two main subsections: theoretical and experimental. The former consists of three parts: bulk properties of FeCrVAl, the effect of Mn and Co substitution, and the effect of external mechanical strain. The paper is summarized in Section IV.

II. Methods

II-1. Computational Methods

The computational results reported in this work are obtained using the Advanced Cyberinfrastructure Coordination Ecosystem (ACCESS) (formerly known as Extreme Science and Engineering Discovery Environment (XSEDE)) resources located at the Pittsburgh Supercomputing Center (PSC)²³, and with the resources of the Center for Functional Nanomaterials (CFN) at Brookhaven National Laboratory (BNL). For all our calculations, we used the Vienna *ab initio* simulation package (VASP),²⁴ within the projector augmented-wave method (PAW)²⁵ and generalized-gradient approximation (GGA).²⁶ The atomic positions are optimized

until the energy difference between consecutive steps is 10^{-5} eV or less. The converging energy difference between the consecutive steps is set to 10^{-3} meV for the electronic structure calculations. We used the integration method by Methfessel and Paxton,²⁷ and we set the cut-off energy to 500 eV. The k-point mesh used for the Brillouin-zone integration is set to $6\times6\times6$ (ionic relaxation), and $12\times12\times12$ (electronic structure calculations). The crystal structures are obtained and visualized using the MedeA® software environment.²⁸ We did not include the Hubbard U correction in our calculations because the considered systems are metallic. In metals, the correlation effects are less important than in magnetic insulators and are usually well described within regular GGA.

The uniform (hydrostatic) pressure is simulated by varying all three lattice parameters by the same amount. At the same time, to simulate the biaxial strain, we kept the in-plane lattice parameters (x and y) fixed, and optimized the out-of-plane lattice constant (z). Thus, only at the equilibrium lattice constant, the considered alloys under biaxial strain are cubic.

II-2. Experimental Methods

FeCrVAl, FeCr_{0.5}Mn_{0.5}VAl, and FeCr_{0.5}Co_{0.5}VAl bulk ingots were prepared using arcmelting and high-vacuum annealing. First, highly pure (99.99%) metal pieces with proper weight ratio were cut from corresponding commercially available pellets and melted on a water-cooled Cu hearth of an arc furnace in an argon environment. The subsequent annealing of each sample was done in a tubular vacuum furnace ($\sim 10^{-7}$ torr) at 600°C for 48 hours to improve the crystalline quality of the samples. The crystal structures of the samples were investigated using Rigaku MiniFlex600 x-ray diffractometer with Cu-K α source (λ = 1.54 Å), and magnetic properties were measured using a Quantum Design VersaLab magnetometer and a Quantum Design DynaCool PPMS with the ACMSII option. Energy-dispersive x-ray spectroscopy (EDS) was used to confirm the elemental compositions of the annealed samples, where the measured compositions were close to the nominal compositions.

III. Results and Discussion

III-1. Theory

III-1-a. Bulk FeCrVAl

Figure 1 shows the crystal structure of FeCrVAl, which we determined by finding the minimum energy configuration in a 16-atom unit cell. In literature, this structure is usually referred to as a regular cubic Heusler structure, prototype Cu₂MnAl.

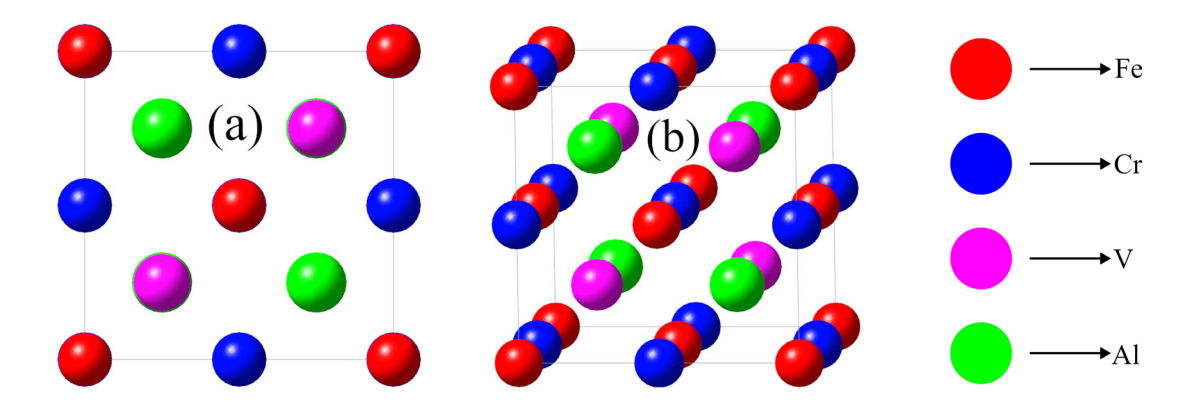


Figure 1: The unit cell of FeCrVAl: top view (a), and side view (b). Atoms are colored as indicated in the Figure, i.e. Fe – red, Cr – blue, V – magenta, Al – light green.

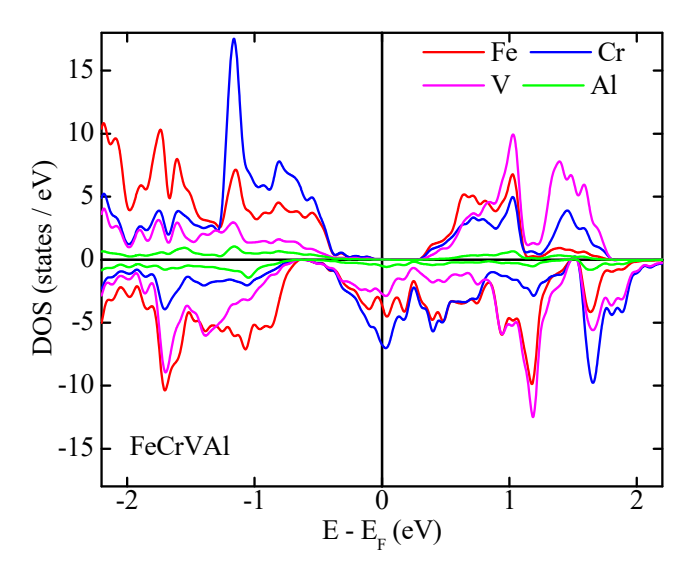


Figure 2: Calculated element- and spin- resolved density of states of bulk FeCrVAl. Color scheme of atomic contributions is indicated in the figure, and is consistent with the one used in Fig. 1.

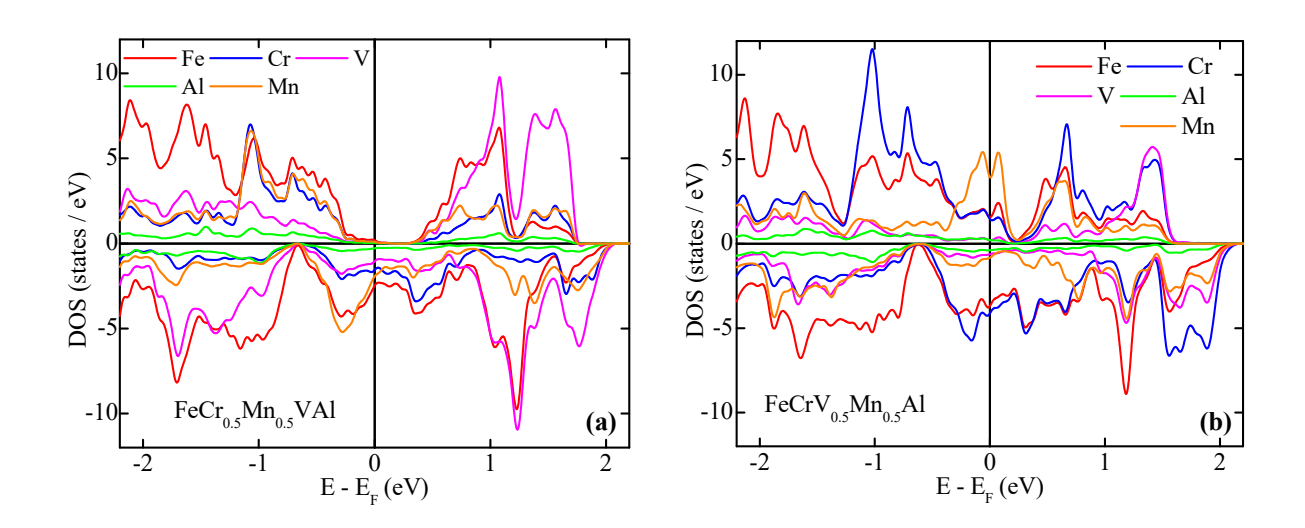
Figure 2 shows the calculated density of states (DOS) of FeCrVAl in the ground state. The calculated equilibrium lattice constant is 5.826 Å, while the calculated total magnetic moment is 2.00 μ_B/f . u. This value is consistent with the Slater-Pauling rule (on the electron-deficient side), according to which the spin magnetic moment per unit cell is given as m = N - 24, where N is the number of valence electrons, which is 22 per 4-atom unit cell of FeCrVAl.²⁹ The magnetic

alignment is ferrimagnetic (see detailed discussion on the magnetic structure below). The calculated spin polarization, P is around 98%. Here, P is defined as $P = \left| \left(N_{\uparrow}(E_F) - N_{\downarrow}(E_F) \right) \middle/ \left(N_{\uparrow}(E_F) + N_{\downarrow}(E_F) \right) \middle|$, where $N_{\uparrow\downarrow}(E_F)$ is the spin-dependent density of states at the Fermi level, E_F .³⁰ These results are consistent with earlier reported data.²²

III-1-b. Bulk FeCr $_{0.5}$ Mn $_{0.5}$ VAl, FeCr $_{0.5}$ Mn $_{0.5}$ Al, FeCr $_{0.5}$ Co $_{0.5}$ VAl, and FeCr $_{0.5}$ Co $_{0.5}$ Al

Figure 3 shows calculated density of states of bulk FeCr_{0.5}Mn_{0.5}VAl (a), FeCrV_{0.5}Mn_{0.5}Al (b), FeCr_{0.5}Co_{0.5}VAl (c), FeCrV_{0.5}Co_{0.5}Al (d), in the ground state. For each of these four compounds the lowest energy atomic configuration was determined, before calculating electronic structure. All reported compounds exhibit cubic symmetry.

The calculated equilibrium lattice constants, magnetic moments and spin polarizations are 5.783 Å, 1.48 μ_B , and 93% for FeCr_{0.5}Mn_{0.5}VAl; 5.770 Å, 1.85 μ_B , and 5.5% for FeCr_{V_{0.5}Mn_{0.5}Al; 5.750Å, 0.47 μ_B , and 94% for FeCr_{0.5}Co_{0.5}VAl; and 5.790 Å, 3.95 μ_B , and 21% for FeCr_{V_{0.5}Co_{0.5}Al, respectively. Because of the small spin polarization of FeCr_{V_{0.5}Mn_{0.5}Al and FeCr_{V_{0.5}Co_{0.5}Al, we do not study this material further in the rest of this work. We also note that the calculated magnetic moments for highly spin polarized FeCr_{0.5}Mn_{0.5}VAl and FeCr_{0.5}Co_{0.5}VAl are close to the ones estimated with the Slater-Pauling rule, while the moments of FeCr_{V_{0.5}Mn_{0.5}Al and FeCr_{V_{0.5}Co_{0.5}Al are not. This is consistent with the fact that FeCr_{0.5}Mn_{0.5}VAl and FeCr_{0.5}Co_{0.5}VAl are nearly half-metallic, while FeCr_{V_{0.5}Mn_{0.5}Al and FeCr_{V_{0.5}Co_{0.5}Al exhibit very small spin polarization.}}}}}}}}



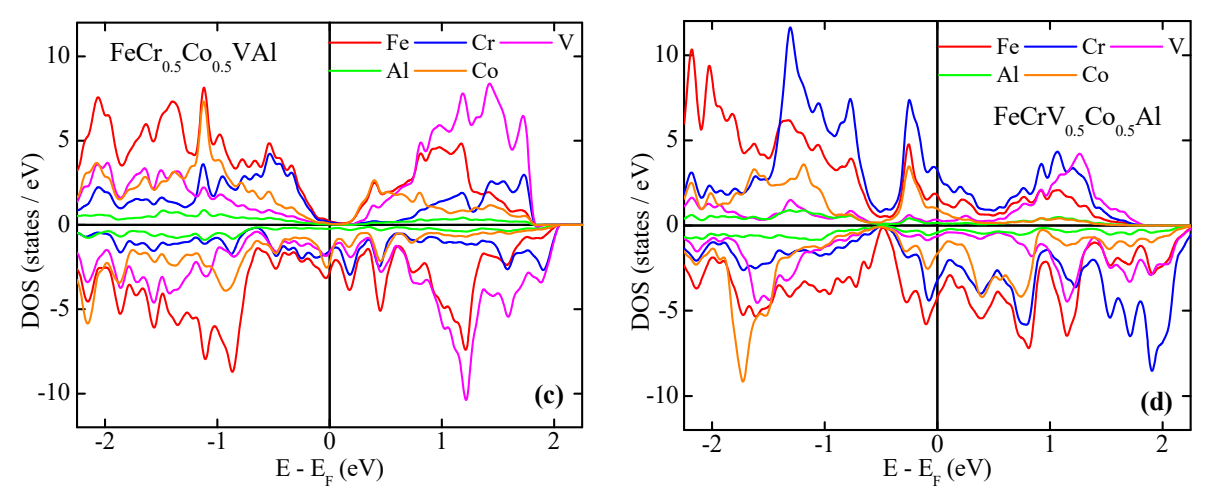


Figure 3: Calculated element- and spin- resolved density of states of bulk FeCr_{0.5}Mn_{0.5}VAl (a), FeCrV_{0.5}Mn_{0.5}Al (b), FeCr_{0.5}Co_{0.5}VAl (c), FeCrV_{0.5}Co_{0.5}Al (d). Color scheme of atomic contributions is indicated in the figure.

III-1-c. Effect of uniform pressure and biaxial strain

For practical device applications, materials are often needed in thin-film geometry, i.e., in multilayer heterostructures. In such cases, the effect of mechanical strain (due to substrate) may often alter the electronic and magnetic properties of materials.³¹ In this section, we analyze the effect of uniform pressure and biaxial strain on FeCrVAl and FeCr_{0.5}Mn_{0.5}VAl. As will be illustrated below, tensile strain may be used to enhance the spin polarization of these materials.

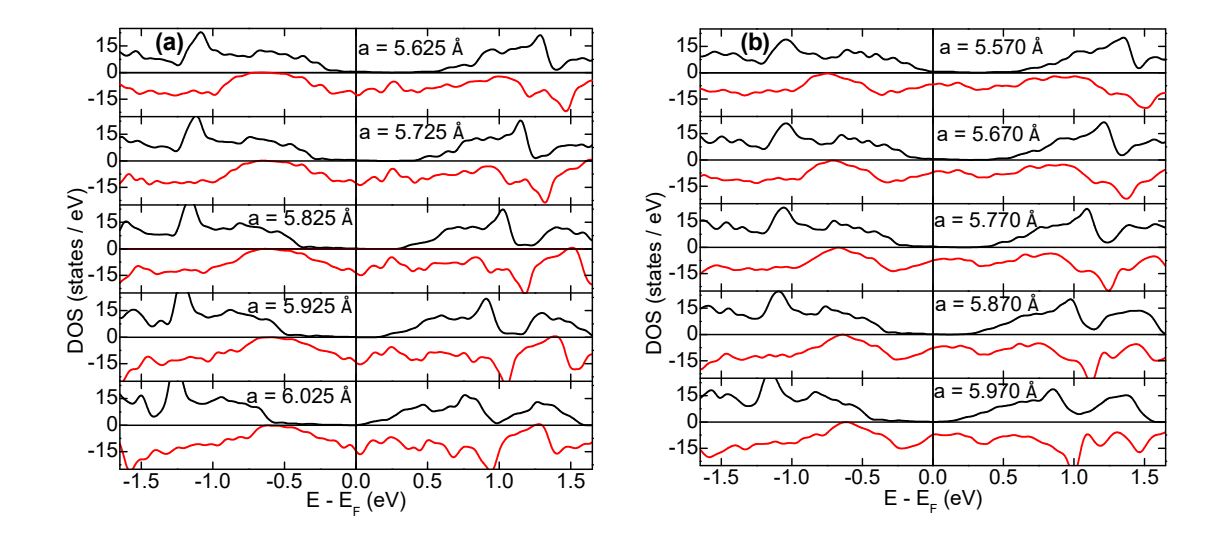


Figure 4: Calculated total DOS of bulk FeCrVAl (a), and bulk FeCr_{0.5}Mn_{0.5}VAl (b) under uniform pressure. Black line – majority-spin, red line – minority-spin. Vertical line corresponds to the Fermi level. Lattice constants at which DOS is calculated are indicated in the figure.

Figure 4 shows calculated total DOS of FeCrVAl and FeCr_{0.5}Mn_{0.5}VAl under uniform pressure. The lattice constants at which the calculations were performed are indicated in the figure. Although it may not be immediately clear from the figure, the application of uniform expansion appears to enhance the spin polarization value of both materials. This issue is addressed in more detail below.

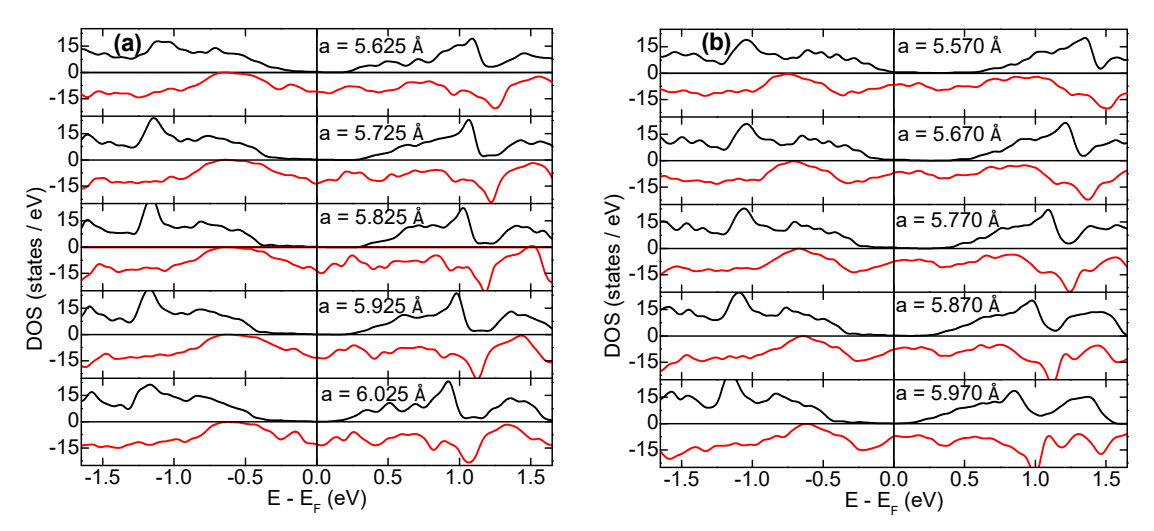


Figure 5: Calculated total DOS of bulk FeCrVAl (a), and bulk FeCr_{0.5}Mn_{0.5}VAl (b) under biaxial strain. Black line – majority-spin, red line – minority-spin. Vertical line at which corresponds to the Fermi level. Lattice constants at which DOS is calculated are indicated in the figure.

Figure 5 shows calculated total DOS of FeCrVAl and FeCr_{0.5}Mn_{0.5}VAl under biaxial strain. The in-plane lattice constants at which the calculations were performed are indicated in the figure. The out-of-plane lattice parameters were fully optimized, and are shown in the Figure 6, as a function of in-plane lattice constants. Again, it may not be immediately clear from Figure 5, but the application of tensile strain slightly enhances the spin polarization of both materials, as discussed in the next paragraph.

Figure 7 shows calculated spin polarization of FeCrVAl (black line and squares) and FeCr_{0.5}Mn_{0.5}VAl (blue line and circles) under uniform pressure (a) and biaxial strain (b). As can be seen from the figure, uniform expansion / tensile strain enhances the spin polarization of both

alloys, and, therefore, may be considered a preferable scenario for practical applications. The enhancement is due to the shift of the Fermi level toward majority-spin energy gap, as can be seen from Figures 4 and 5.

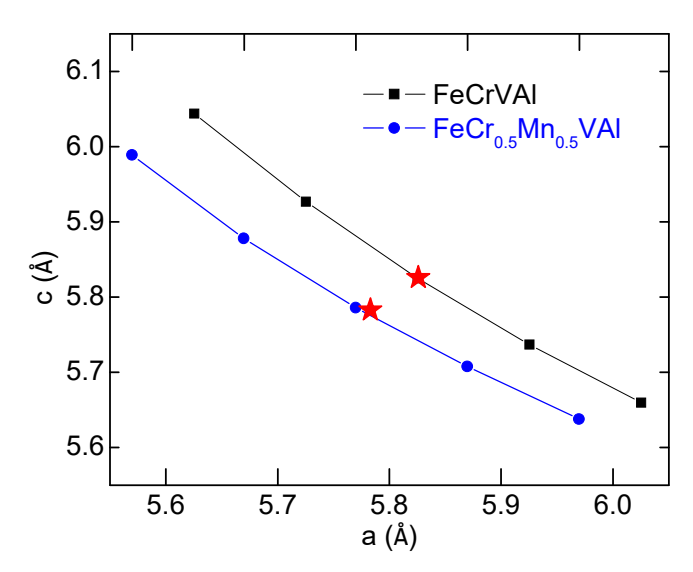


Figure 6: Calculated out-of-plane vs. in-plane lattice constants of FeCrVAl (black line and squares) and FeCr_{0.5}Mn_{0.5}VAl (blue line and circles) under biaxial strain. Red stars indicate the equilibrium lattice parameters, which correspond to the cubic cells.

Figure 8 shows calculated total magnetic moment (in units of μ_B / f.u.) of FeCrVAl (black line and squares) and FeCr_{0.5}Mn_{0.5}VAl (blue line and circles) under uniform pressure (a) and biaxial strain (b). As can be seen from the figure, uniform expansion / tensile strain enhances the magnetization of both alloys, although for tensile strain this effect is fairly small (note the scale of the y-axis). The enhancement of magnetization is largely due to the increase of the Cr magnetic moment under expansion of the unit cell volume. This is illustrated in Figure 9, which shows calculated magnetic moment per atom of FeCrVAl under uniform pressure (a) and biaxial strain (b); and magnetic moment of FeCr_{0.5}Mn_{0.5}VAl under uniform pressure (c) and biaxial strain (d). This figure also illustrates the ferrimagnetic nature of these alloys, due to the vanadium magnetic moments being anti-parallel to those of Cr, Fe, and Mn (magnetic moment of Al is negligible).

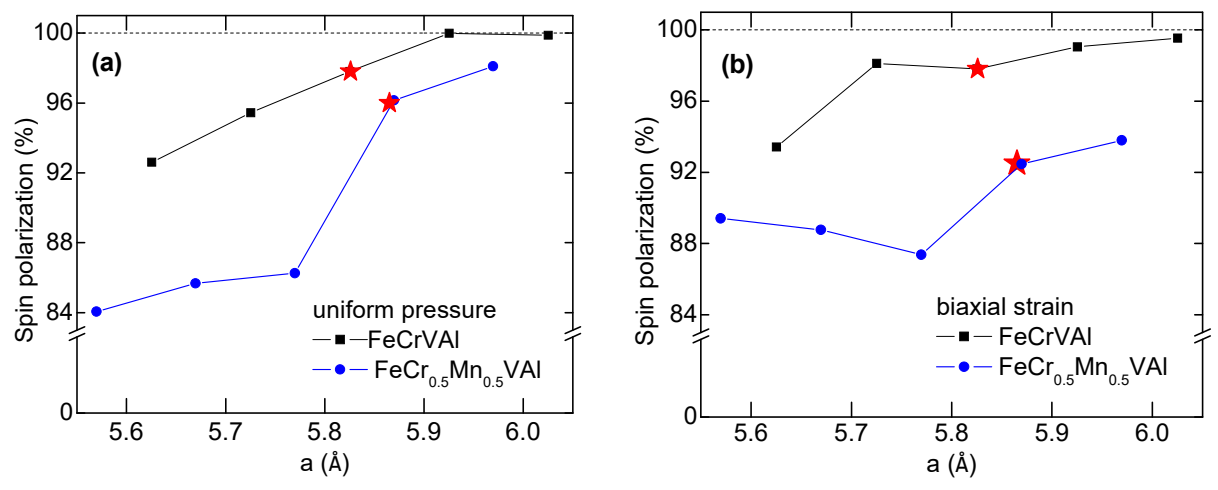


Figure 7: Spin polarization of FeCrVAl (black line and squares) and FeCr_{0.5}Mn_{0.5}VAl (blue line and circles) under uniform pressure (a) and biaxial strain (b) as a function of in-plane lattice constant. Dashed horizontal line indicates 100% spin polarization. Red stars indicate the equilibrium lattice parameters, which correspond to the cubic cells.

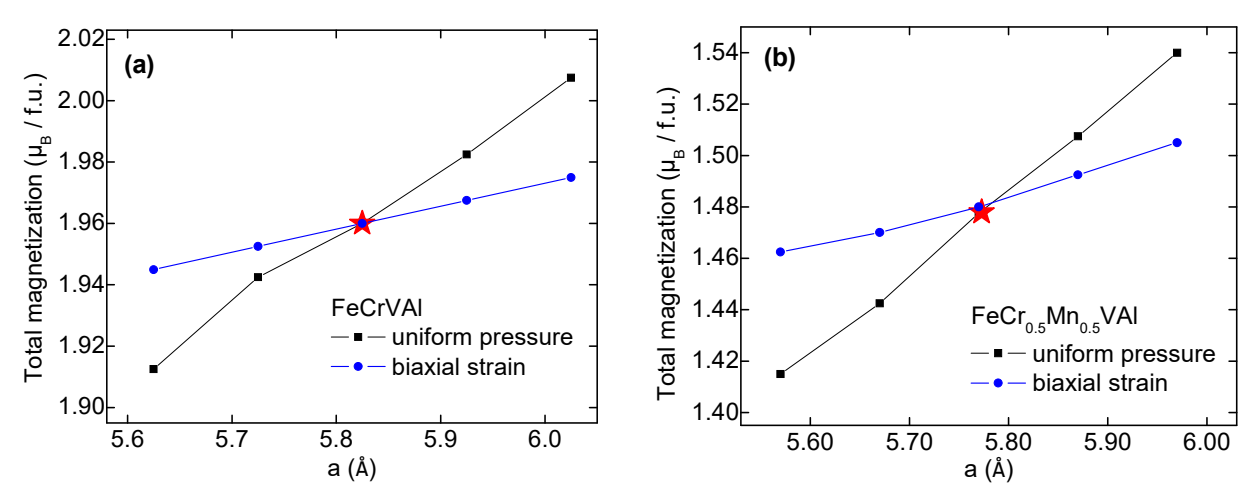


Figure 8: Total magnetization of FeCrVAl (a) and FeCr_{0.5}Mn_{0.5}VAl (b) under uniform pressure (black line and squares) and biaxial strain (blue line and circles). Red stars indicate the equilibrium lattice parameters, which correspond to the cubic cells.

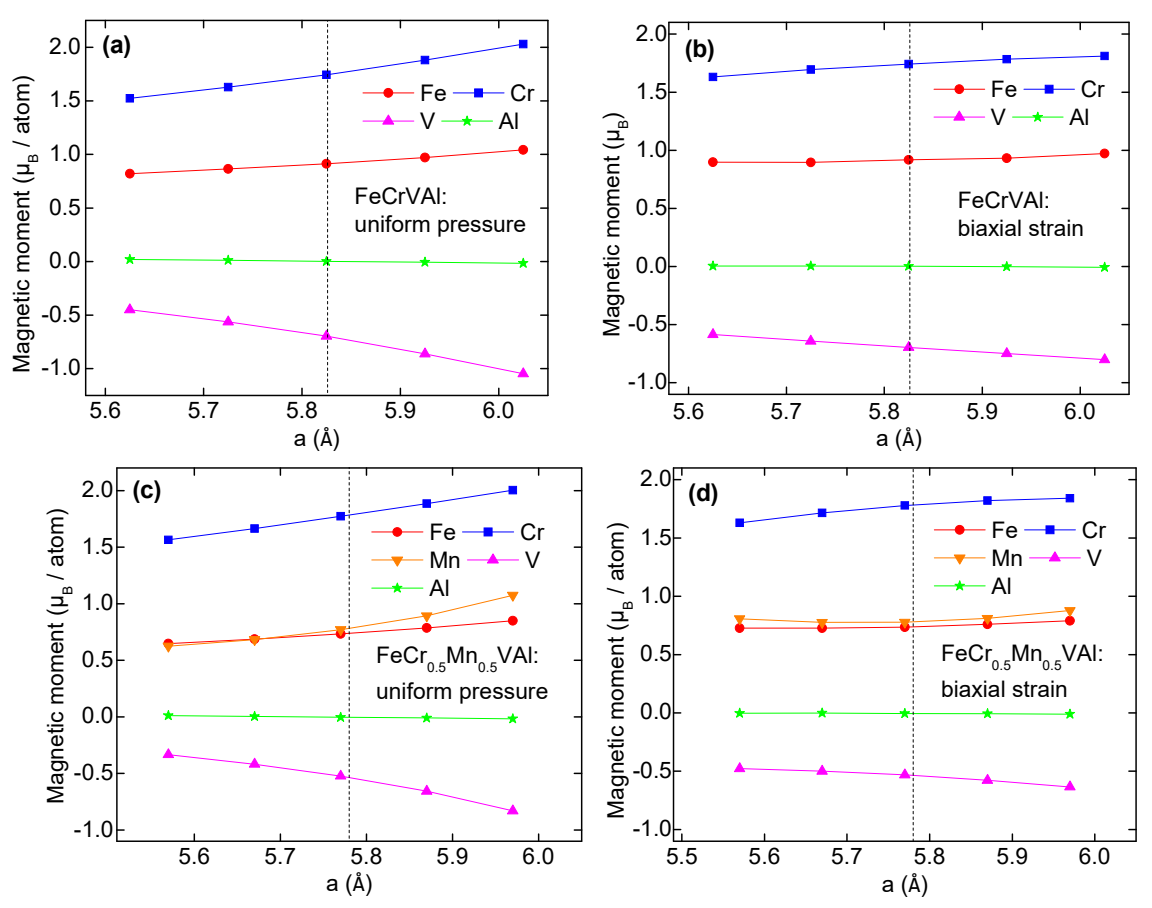


Figure 9: Magnetic moment per atom of FeCrVAl under uniform pressure (a) and biaxial strain (b); and magnetic moment of FeCr_{0.5}Mn_{0.5}VAl under uniform pressure (c) and biaxial strain (d). Atoms are labeled and colored as indicated in the Figure. Vertical dashed line indicates the position of the equilibrium lattice parameter.

III-2. Experiment

Figure 10 shows the x-ray diffraction patterns of FeCrVAl, FeCr_{0.5}Co_{0.5}VAl and FeCr_{0.5}Mn_{0.5}VAl alloys recorded at room temperature. The XRD patterns suggest that all three alloys crystallized in the cubic structure with small amount of impurity phase. Since the intensities of (111) and (200) superlattice peaks are very weak, there is significant disorder in all three samples. The Rietveld analysis of the XRD plots suggest that there is less than 10 wt. % of FeO₂ impurity in all three samples. The lattice parameters extracted from the Rietveld analysis are 5.859 Å, 5.830 Å, and 5.810 Å respectively. These values are close to the lattice parameters predicted by our first principles calculations. In addition, FeCrVAl, FeCr_{0.5}Co_{0.5}VAl and FeCr_{0.5}Mn_{0.5}VAl also contain 5 wt.%, 7 wt.% and 8 wt.% of FeO₂ impurity phase. The simulations were modeled

by assuming a full B2 type disorder where V and Al share 50:50 between their sites. For the Mn and Co doped samples, it is assumed that the dopants occupy Cr sites. However, because of closeness of atomic numbers of V, Cr, Mn, Fe and Co, it is very difficult to precisely identify the site occupancy using Rietveld analysis.

Figure 11 shows the magnetization as a function of magnetic field of (a) FeCrVAl, (b) FeCr_{0.5}Co_{0.5}VAl, and (c) FeCr_{0.5}Mn_{0.5}VAl alloys measured at 5 K. The M (H) curves of FeCrVAl and FeCr_{0.5}Co_{0.5}VAl are almost linear with no saturation. The magnetization measured at 9 T are respectively 1.5 emu/g (0.05 μ_B / f. u) and 0.7 emu/g (0.02 μ_B / f.u). However, the M(H) curve of FeCr_{0.5}Mn_{0.5}VAl is similar to that of a ferromagnetic or ferrimagnetic material with saturation magnetization of 15 emu/g (0.51 μ_B / f.u). All these high-field magnetizations are much smaller than the theoretically predicted values. We attribute this discrepancy to the observed structural disorder as seen in the XRD patterns, which was not considered in our calculations.

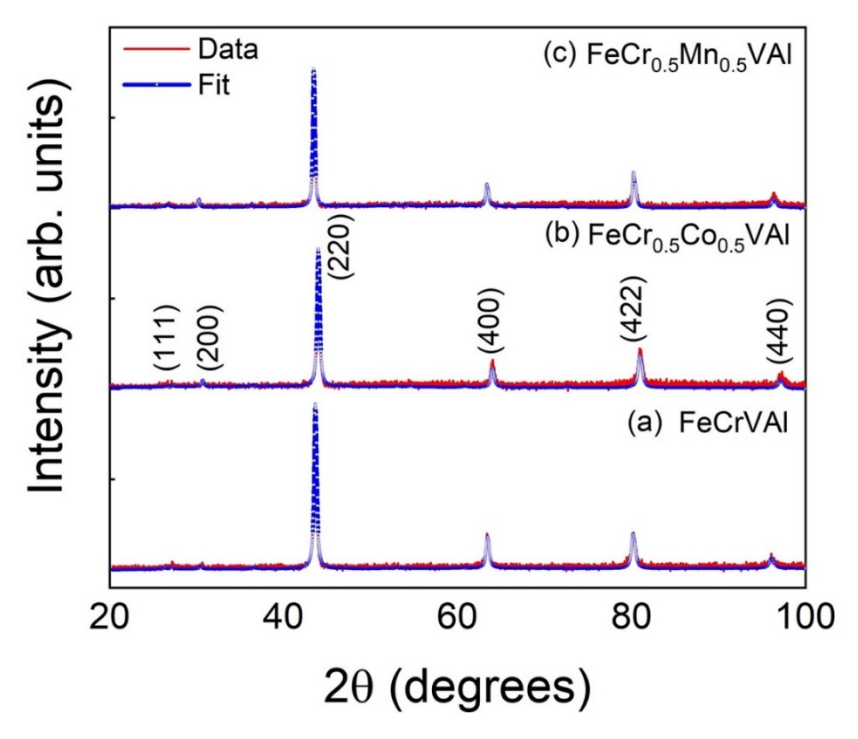


Figure 10: Room temperature x-ray diffraction patterns of (a) FeCrVAl, (b) FeCr_{0.5}Co_{0.5}VAl, and (c) FeCr_{0.5}Mn_{0.5}VAl Heusler alloys.

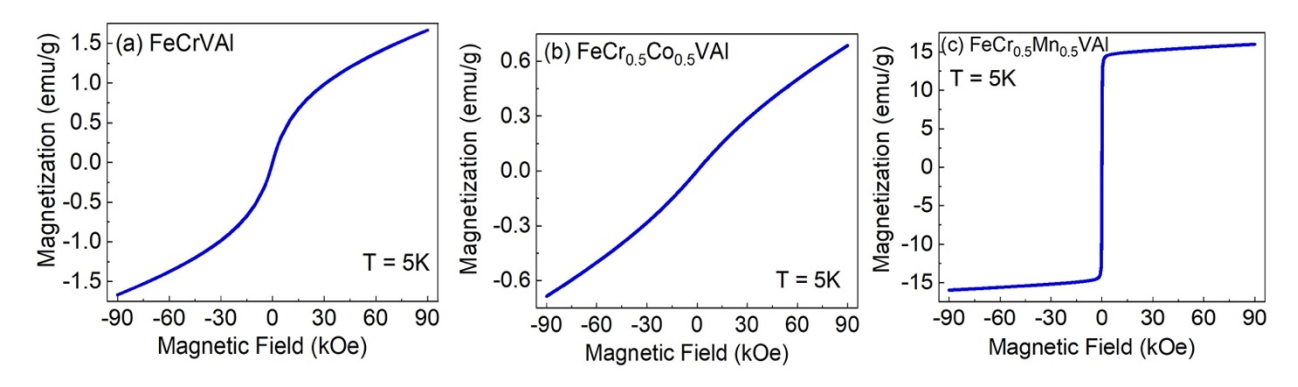


Figure 11: The isothermal magnetic curves M(H) of (a) FeCrVAl, (b) FeCr_{0.5}Co_{0.5}VAl, and (c) FeCr_{0.5}Mn_{0.5}VAl Heusler alloys.

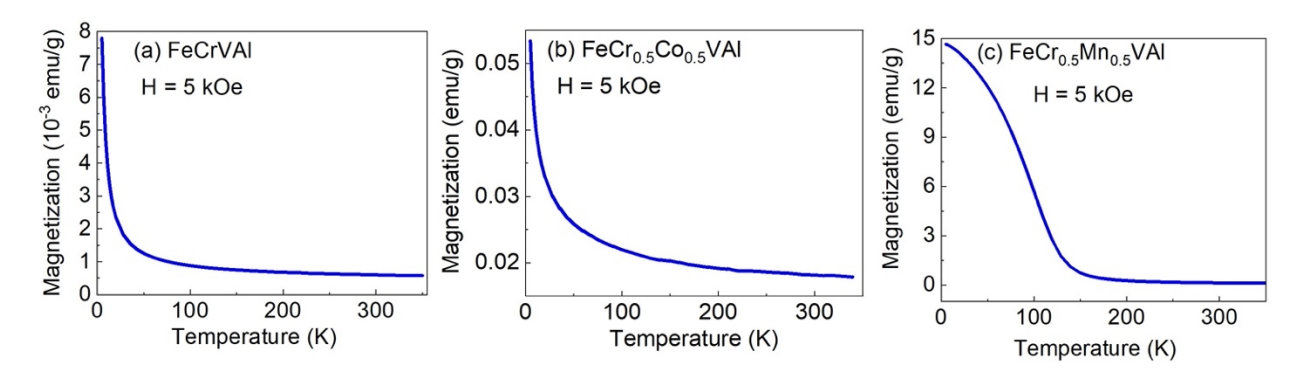


Figure 12: The thermomagnetic curves M(T) of (a) FeCrVAl, (b) FeCr_{0.5}Co_{0.5}VAl, and (c) FeCr_{0.5}Mn_{0.5}VAl Heusler alloys.

Figure 12 shows the magnetization as a function of temperature of (a) FeCrVAl, (b) FeCr_{0.5}Co_{0.5}VAl, and (c) FeCr_{0.5}Mn_{0.5}VAl alloys measured at 5 kOe. The M(T) curves of FeCrVAl and FeCr_{0.5}Co_{0.5}VAl are similar to those of paramagnetic materials. However, the M(T) curve of FeCr_{0.5}Mn_{0.5}VAl resembles with that of a ferrimagnetic (or ferromagnetic) material with the Curie temperature of 135 K.

IV. Conclusions

In conclusion, we performed a comprehensive theoretical study of FeCrVAl, FeCr_{0.5}Mn_{0.5}VAl, FeCr_{0.5}Mn_{0.5}VAl, FeCr_{0.5}Co_{0.5}VAl, and FeCr_{0.5}Co_{0.5}VAl; and experimental study of FeCrVAl, FeCr_{0.5}Mn_{0.5}VAl, and FeCr_{0.5}Co_{0.5}VAl Heusler alloys. Our results indicate that FeCr_{0.5}Mn_{0.5}VAl, and FeCr_{0.5}Co_{0.5}VAl alloys exhibit high values of spin-polarization,

above 90%. Application of tensile strain may enhance these values, essentially making these materials half-metallic. According to our calculations, this enhancement is due to the shift of the Fermi level toward majority-spin energy gap. The magnetic alignment of these alloys is ferrimagnetic, with a moderate value of total magnetization. More specifically, the ferrimagnetic alignment is manifested by vanadium magnetic moments being anti-parallel to those of Cr, Fe, and Mn. Our measured magnetization values are smaller than the theoretically predicted ones. This discrepancy is likely due to the observed structural disorder. Although our theoretical calculations predict high spin polarizations for three of the studied alloys, it is necessary to develop disorder free materials for spin transport-based device applications.

Acknowledgments

This research is supported by the *National Science Foundation* (NSF) under Grant Numbers 2003828 and 2003856 via DMR and EPSCoR. This work used the Advanced Cyberinfrastructure Coordination Ecosystem (ACCESS) (formerly known as Extreme Science and Engineering Discovery Environment (XSEDE)), which is supported by National Science Foundation grant number ACI-1548562. This work used the XSEDE Regular Memory (Bridges 2) and Storage (Bridges Ocean) at the Pittsburgh Supercomputing Center (PSC) through allocation TG-DMR180059, and the resources of the Center for Functional Nanomaterials, which is a U.S. DOE Office of Science Facility, and the Scientific Data and Computing Center, a component of the Computational Science Initiative, at Brookhaven National Laboratory (BNL) under Contract No. DE-SC0012704.

References

¹ R. A. de Groot, F. M. Mueller, P. G. van Engen, and K. H. J. Buschow, Phys. Rev. Lett. **50**, 2024 (1983).

² I. Galanakis, P. H. Dederichs, N. Papanikolaou, Phys. Rev. B **66**, 174429 (2002).

³ E. Şaşıoğlu, L. M. Sandratskii, and P. Bruno, Phys. Rev. B **72**, 184415, (2005).

⁴ B. Balke, G. H. Fecher, J. Winterlik, and C. Felser, Appl. Phys. Lett. **90**, 152504 (2007).

⁵ H. Kurt, K. Rode, M. Venkatesan, P. Stamenov, and J. M. D. Coey, Phys. Status Solidi B **248**, 2338 (2011).

J. Winterlik, S. Chadov, A. Gupta, V. Alijani, T. Gasi, K. Filsinger, B. Balke, G. H. Fecher, C. A. Jenkins, F. Casper, J. Kübler, G. Liu, L. Gao, S. S. P. Parkin, and C. Felser, Adv. Mater. 24, 6283 (2012).

⁷ I. Galanakis, in *Heusler Alloys*, Springer Series in Materials Science 222, C. Felser and A. Hirohata (eds.), Springer International Publishing Switzerland 2016.

- ⁸ S. Ouardi, G. H. Fecher, and C. Felser, Phys. Rev. Lett. **110**, 100401 (2013).
- P. Lukashev, P. Kharel, S. Gilbert, B. Staten, N. Hurley, R. Fuglsby, Y. Huh, S. Valloppilly, W. Zhang, K. Yang, R. Skomski, and D. J. Sellmyer, Appl. Phys. Lett. 108, 141901 (2016).
- ¹⁰ R. Carlile, J. Herran, S. Poddar, E. Montgomery, P. Kharel, P. Shand and P. Lukashev, J. Phys.: Condens. Matter **33**, 105801 (2021).
- ¹¹ L. Stuelke, P. Kharel, P. Shand, and P. Lukashev, Phys. Scr. **96**, 125818 (2021).
- ¹² F.B. Mancoff, B.M. Clemens, E.J. Singley, D.N. Basov, Phys. Rev. B **60**(R12) 565 (1999).
- ¹³ W. Zhu, B. Sinkovic, E. Vescovo, C. Tanaka, J.S. Moodera, Phys. Rev. B **64**, R060403 (2001).
- ¹⁴ A.N. Caruso, C.N. Borca, D. Ristoiu, J.P. Nozieres, P.A. Dowben, Surf. Sci. **525**, L109 (2003).
- D. Ristoiu, J.P. Nozières, C.N. Borca, B. Borca, P.A. Dowben, Appl. Phys. Lett. 76, 2349 (2000).
- ¹⁶ I. Galanakis, J. Phys. Condens. Matter **14**, 6329 (2002).
- ¹⁷ M. Ležaic, I. Galanakis, G. Bihlmayer, S. Blügel, J. Phys. Condens. Matter 17, 3121 (2005).
- P. Kharel, W. Zhang, R. Skomski, S. Valloppilly, Y. Huh, R. Fuglsby, S. Gilbert, and D. J. Sellmyer, Phys. D: Appl. Phys. 48, 245002 (2015).
- ¹⁹ J. Herran, R. Dalal, P. Gray, P. Kharel, and P. Lukashev; J. Appl. Phys., **122**, 153904 (2017).
- ²⁰ G. A. de Wijs and R. A. de Groot, Phys. Rev. B **64**, 020402(R) (2001).
- A. Debernardi, M. Peressi, and A. Baldereschi, Mater. Sci. Eng. C 23, 743 (2003).
- ²² R. Dhakal, S. Nepal, I. Galanakis, R.P. Adhikari, G.C. Kaphle, Journal of Alloys and Compounds **882**, 160500 (2021).
- J. Towns, T. Cockerill, M. Dahan, I. Foster, K. Gaither, A. Grimshaw, V. Hazlewood, S. Lathrop, D. Lifka, G. D. Peterson, R. Roskies, J. R. Scott, N. Wilkins-Diehr, "XSEDE: Accelerating Scientific Discovery", Computing in Science & Engineering, vol.16, no. 5, pp. 62-74, Sept.-Oct. 2014.
- ²⁴ G. Kresse and D. Joubert, Phys. Rev. B **59**, 1758 (1999).
- ²⁵ P. Blöchl, Phys. Rev. B **50**, 17953 (1994).
- ²⁶ J. P. Perdew, K. Burke, and M. Ernzerhof, Phys. Rev. Lett. 77, 3865 (1996).
- ²⁷ M. Methfessel and A. T. Paxton, Phys. Rev. B **40**, 3616 (1989).
- ²⁸ MedeA-2.22, Materials Design, Inc., San Diego, CA, USA, 2017.
- ²⁹ G. Fecher, H. Kandpal, S. Wurmehl, C. Felser, G. Schönhense. J. Appl. Phys. 99, 08J106 (2006).
- ³⁰ J. P. Velev, P. A. Dowben, E. Y. Tsymbal, S. J. Jenkins, and A. N. Caruso, Surf. Sci. Rep. **63**, 400 (2008).
- ³¹ I. Tutic, J. Herran, B. Staten, P. Gray, T. Paudel, A. Sokolov, E. Tsymbal, and P. Lukashev, J. Phys.: Condens. Matter **29**, 075801 (2017).